FORMATION OF DIFFERENT ISOTOPOMERS OF CHLORONIUM IN THE INTERSTELLAR MEDIUM

Liton Majumdar[1], Ankan Das[1], and Sandip K. Chakrabarti[2,1]
[1] Indian Centre for Space Physics, Chalantika 43, Garia Station Road, Kolkata, 700084, India; ankan.das@gmail.com
[2] S. N. Bose National Centre for Basic Sciences, Salt Lake, Kolkata, 700098, India

ABSTRACT

The main focus of this paper is to explore the possibility of finding two deuterated isotopomers of H_2Cl^+ (chloronium) in and around the interstellar medium. The presence of a chloronium ion has recently been confirmed by the *Herschel Space Observatory*'s Heterodyne Instrument for the far-infrared. It observed para-chloronium toward six sources in the Galaxy. To date the existence of its deuterated isotopomers ($HDCl^+$ and D_2Cl^+) have not been discussed in the literature. We find that these deuterated gas phase ions could be destroyed by various ion–molecular reactions, dissociative recombination (DR), and cosmic rays (CRs). We compute all of the ion–molecular (polar) reaction rates by using the parameterized trajectory theory and the ion–molecular (non-polar) reaction rates by using the Langevin theory. For DR- and CR-induced reactions, we adopt two well-behaved rate formulas. We also include these rate coefficients in our large gas–grain chemical network to study the chemical evolution of these species around the outer edge of the cold, dense cloud. In order to study spectral properties of the chloronium ion and its two deuterated isotopomers, we have carried out quantum chemical simulations. We calculated ground-state properties of these species by employing second-order Moller–Plesset perturbation theory (MP2) along with quadruple-zeta correlation consistent (aug-cc-pVQZ) basis set. Infrared and electronic absorption spectra of these species are calculated by using the same level of theory. The MP2/aug-cc-pVQZ level of theory is used to report the different spectroscopic constants of these gas phase species. These spectroscopic constants are essential to predict the rotational transitions of these species. Our predicted column densities of D_2Cl^+, $HDCl^+$, along with spectral information may enable their future identification around outer edges of cold, dark clouds.

Key words: astrochemistry – evolution – ISM: abundances – ISM: clouds – ISM: molecules – methods: numerical – molecular data

1. INTRODUCTION

The Cologne Database for Molecular Spectroscopy catalog (Müller et al. 2001; Müller et al. 2005) keeps records on discovered molecules in the interstellar medium (ISM). According to this catalog, more than 170 molecules have been detected so far in the ISM. Among them are some simple halides, such as HF, CF, AlF, HCl, HCl^+, NaCl, KCl, AlCl, and MgCl. Several works have been done in the past to model the chemistry of the chlorine-bearing molecules in both the diffuse and dense molecular clouds (Jura 1974; Dalgarno et al. 1974; van Dishoeck & Black 1986; Schilke et al. 1995; Federman et al. 1995; Amin 1996; Neufeld & Wolfire 2009). Various halogen elements, such as fluorine and chlorine, having solar abundances (3.6×10^{-8} and 3.2×10^{-7}, respectively, relative to total hydrogen nuclei; Asplund et al. 2009) play an important role toward the formation of various hydrides in the ISM. Dissociation energy of most of the hydrides are less than that of the hydrogen molecule; the only exceptions are the diatomic hydrides, such as HF, and diatomic hydride cations, such as HCl^+ (Lis et al. 2010). Around an ISM, most of the halogen elements are biased to form hydrides (Neufeld et al. 2010). Huge abundances of HF and H_2Cl^+ are observed around the diffuse molecular clouds (Neufeld et al. 2010; Sonnentrucker et al. 2010; Lis et al. 2010).

The ionization potential of chlorine is slightly less than that of hydrogen and singly ionized chlorine (Cl^+) can react exothermically with H_2 to form HCl^+. This HCl^+ further interacts with H_2 to form H_2Cl^+. These features are already known by theory of thermochemistry of these species. Since the chloronium ion does not react with the hydrogen molecule, dissociative recombination (DR) appears to be its main destruction route. The chloronium ion could also be destroyed by reacting with the CO molecule. The main product of these destruction routes is hydrogen chloride (HCl). Theoretical modeling, by considering the chlorine-bearing molecules, predicts that abundances of the chloronium ions are significantly higher and could be observed. But surprisingly, before the launching of *Herschel*, among the Cl-bearing molecules, only $H^{35}Cl$ and $H^{37}Cl$ were detected (Blake et al. 1985; Zmuidzinas et al. 1995; Schilke et al. 1995; Salez et al. 1996). Chemical modeling suggests that chloronium ions could be very abundant around the diffuse ISM. The detection of H_2Cl^+ was first reported toward NGC 6334I and Sgr B2(S) using the Heterodyne Instrument for Far-Infrared (HIFI; de Graauw et al. 2010) aboard the *Herschel Space Observatory* (Pilbratt et al. 2010). A follow-up study by Neufeld et al. (2012) also detected H_2Cl^+ absorption toward Sgr A, W31C and detected chloronium emission from two sources in the Orion Molecular Cloud 1 (the Orion Bar photodissociation region and Orion South condensation) and the young massive star, AFGL 2591.

Despite the overwhelmingly significant observational evidence, to date, no deuterated forms of H_2Cl^+ have been observed in the ISM. This motivates us to model the formation/destruction of different forms of deuterated H_2Cl^+ in the ISM. The importance of interstellar grains in producing simpler molecules has been widely described by several authors such as Allen & Robinson (1977), Cazaux et al. (2010), Cuppen & Herbst (2007), Stantcheva et al. (2002), Hasegawa et al. (1992), Chakrabarti et al. (2006a, 2006b), Das et al. (2008a, 2008b, 2010), and Das & Chakrabarti (2011). These studies indicate that dusts could play a crucial role in deciding chemical compositions around any molecular cloud. In order to

understand the complete picture of how molecules are formed in or around an ISM, we used our large gas–grain chemical model (Chakrabarti & Chakrabarti (2000a, 2000b); Das et al. 2013a; Majumdar et al. 2012, 2013a, 2013b).

Majumdar et al. (2013a, 2013b) and Das et al. (2013b) performed quantum chemical simulations to find out various chemical properties of some interstellar species. In the current paper, we carry out similar types of quantum chemical calculations to find out the spectral information (infrared, electronic, and rotational) of different deuterated isotopomers of the chloronium ion. We have also provided detailed information about rotational transitions of these species (in the format of a JPL catalog). Such a study would be extremely helpful for the identification of these species around ISMs.

The plan of this paper is as follows. In Section 2, the models and the computational details are presented. Implications of the results are discussed in Section 3. Finally, in Section 4, we draw our conclusions. In the Appendix, we tabulate relevant parameters for rotational spectroscopy of one of the isotopomers of H_2Cl^+ in the format of a JPL catalog.

2. COMPUTATIONAL DETAILS

2.1. Quantum Chemical Simulations and Derived Spectral Parameters

We study spectral properties of interstellar chloronium by first optimizing the geometry of chloronium using the second-order Moller–Plesset perturbation theory (MP2) along with a quadruple-zeta correlation consistent (aug-cc-PVQZ) basis set. MP2 theory is a special case of the more general many-body perturbation theory (Puzzarini et al. 2010). For calculations where only valence electrons are correlated (i.e., frozen core calculation), standard cc-pVXZ sets with $X = D$, T, Q, 5, and 6 are recommended (Puzzarini et al. 2010). Because of this, we use the aug-cc-pVQZ basis set along with the MP2 method. Vibrational frequencies of H_2Cl^+ and its two deuterated isotopomers, D_2Cl^+ and $HDCl^+$, are computed by determining the second derivative of energy with respect to Cartesian nuclear coordinates and then transforming it into mass-weighted coordinates. This transformation is valid only at a stationary point.

Vibrational frequencies of these species in the ice phase are also obtained by using the same level of theory. Vibrational spectra of any chemical species are significantly affected by the type of solvent used in the simulation. For our modeling purpose here, we have used the Polarizable Continuum Model (PCM) with an integral equation formalism variant (IEFPCM) as a default Self-Consistent Reaction Field (SCRF) method (Tomasi et al. 2002, 2005, 1999; Pascual-Ahuir et al. 1994). The SCRF method in the Gaussian 09W program is used to perform calculations in the presence of a solvent by placing the solute in a cavity within a solvent reaction field. Following Das et al. (2013b), here too we have considered simple as well as mixed ice. By simple ice, we mean ice made from water molecules only and by mixed ice, we mean ice made from water, methanol, and carbon dioxide. Observations around the cold dense region of the molecular cloud reveal that ∼90% of the interstellar grain mantle could be covered by H_2O, CH_3OH, and CO_2 (Keane et al. 2001). We have also carried out a quantum chemical simulation (time-dependent density functional theory) to find the electronic absorption spectrum of these species in the gas phase as well as simple ice and mixed ice phase using the IEFPCM model.

An important key for the successful identification of different forms of chloronium in the interstellar space depends on the availability of accurate predictions of spectroscopic constants (rotational and distortional constants). Our computed rotational spectral information for interstellar chloronium is based on equilibrium geometry obtained at MP2/aug-cc-pVQZ level, i.e., with the consideration of core correlation and vibrational corrections to the rotational constants. Centrifugal distortion constants are computed from harmonic and anharmonic force fields obtained at MP2/aug-cc-pVQZ levels of theory. In addition, computed components of a dipole moment were used to predict relative intensities of rotational transitions. These spectroscopic constants are essential to predict the spectrum of different forms of H_2Cl^+, and this can be done by following the techniques described in Das et al. (2013b). They used Picket's "SPCAT" program (Pickett et al. 1991) for this purpose. Two main files, namely, "file.var" and "file.int," are required for the SPCAT program. The specified format of these two files were explained in detail in Pickett et al. (1991). Information regarding rotational constants, quadrupole coupling constants, and distortional constants are given in the ".var" file. Contents of the ".var" file could directly be generated from the Gaussian 09 program. The ".int" file is the intensity file, and it is prepared according to the prescribed format of the "SPCAT program." This file contains the maximum and minimum number of rotational states, partition function, rotational temperature, and dipole moment of the molecule.

2.2. Chemical Modeling

In order to study various forms of chloronium in an ISM, we have developed a chemical model which includes a gas phase as well as a grain surface chemical network. Our gas phase chemical network consists of a network of Woodall et al. (2007) and deuterated network used in Das et al. (2013b). In addition, we include some deuterated reactions by following Roberts & Millar (2000) and Albertsson et al. (2013). We include certain new reactions for the formation and destruction of various forms of chloronium and its related species. Our present gas-phase chemical network consists of 6180 reactions, and our present surface chemical network consists of 285 reactions. Except for molecular hydrogen and helium, depletion of all gas phase neutral species onto the grain surface are considered with a sticking probability of unity. The reason for ignoring this for H_2 and He is that according to Leitch & Williams (1985), the sticking coefficient of $H_2 \sim 0b$ and Roberts & Millar (2000) argued that helium would not stick to the grain at all. Next, the list of reactions which are considered in our network for the formation/destruction of deuterated isotopomers of chloronium ion is discussed.

$$H^+ + DCl \rightarrow DCl^+ + H \quad \text{(A1)}$$

$$He^+ + DCl \rightarrow Cl^+ + He + D \quad \text{(A2)}$$

$$C^+ + DCl \rightarrow CCl^+ + D \quad \text{(A3)}$$

$$CH_3^+ + DCl \rightarrow H_2CCl^+ + HD \quad \text{(A4)}$$

$$NH_2D + CCl^+ \rightarrow HCNH^+ + DCl \quad \text{(A5)}$$

$$H_2O + HDCl^+ \rightarrow DCl + H_3O^+ \quad \text{(A6)}$$

$$CO + HDCl^+ \rightarrow DCl + HCO^+ \quad \text{(A7)}$$

$$H_2 + DCl^+ \rightarrow HDCl^+ + H \quad \text{(A8)}$$

$$H_3^+ + DCl \rightarrow HDCl^+ + H_2 \quad \text{(A9)}$$

$$CH_5^+ + DCl \rightarrow HDCl^+ + CH_4 \quad \text{(A10)}$$

$$HD + DCl^+ \rightarrow D_2Cl^+ + H \quad \text{(A11)}$$

$$H_2D^+ + DCl \rightarrow D_2Cl^+ + H_2 \quad \text{(A12)}$$

$$HD_2^+ + DCl \rightarrow D_2Cl^+ + HD \quad \text{(A13)}$$

$$CH_4D^+ + DCl \rightarrow D_2Cl^+ + CH_4 \quad \text{(A14)}$$

$$H_2O + D_2Cl^+ \rightarrow DCl + H_2DO^+ \quad \text{(A15)}$$

$$CO + D_2Cl^+ \rightarrow DCl + DCO^+ \quad \text{(A16)}$$

$$HD + Cl^+ \rightarrow DCl^+ + H \quad \text{(A17)}$$

$$D_2 + Cl^+ \rightarrow DCl^+ + D \quad \text{(A18)}$$

$$H_2 + DCl^+ \rightarrow HDCl^+ + H \quad \text{(A19)}$$

$$HD + HCl^+ \rightarrow HDCl^+ + H \quad \text{(A20)}$$

$$D_2 + HCl^+ \rightarrow HDCl^+ + D \quad \text{(A21)}$$

$$H_2D^+ + Cl \rightarrow DCl^+ + H_2 \quad \text{(A22)}$$

$$HD_2^+ + Cl \rightarrow DCl^+ + HD \quad \text{(A23)}$$

$$D_3^+ + Cl \rightarrow DCl^+ + D_2. \quad \text{(A24)}$$

Reaction A1 is a charge-exchange-type reaction. The rate coefficient for this reaction is assumed to be similar to the rate coefficient adopted for $H^+ + HCl \rightarrow HCl^+ + H$ in Woodall et al. (2007). Reactions (A2)–(A24) are ion–neutral-type reactions. According to Herbst (2006), rate coefficients for ion–molecular reactions can be determined by using capture theories (in which translational energy of reactants must only surpass a long-range centrifugal barrier for a reaction to occur). The collision rate coefficient between an ion and non-polar neutral molecule can be determined by using a so-called Langevin collision rate:

$$k = 2\pi e\sqrt{\alpha_d/\mu}, \quad (1)$$

where, e is the electronic charge, α_d is the polarizability of a neutral non-polar molecule, and μ is the reduced mass of reactants. But for polar neutral species, a complex situation arises due to the attraction between a charge and a rotating permanent dipole moment. In these cases, extensive trajectory calculations have been carried out by Su & Chesnavich (1982) to predict rate coefficients ($k_{\rm cap}$) of ion–polar molecule capture collisions. According to Woon & Herbst (2009), the Su–Chesnavich formula can be written in two different ways, both of which use a parameter, $x = \mu_D/\sqrt{(2\alpha kT)}$, where k is Boltzmann constant and T is the temperature. The ion–dipole ($k_{\rm cap}$) rates can be parameterized using the following equations:

$$k_{\rm cap} = (0.4767x + 0.6200)k_L \quad (2)$$

and

$$k_{\rm cap} = [(x + 0.5090)^2/10.526 + 0.9754]k_L. \quad (3)$$

Equation (2) is used if $x \geqslant 2$ and Equation (3) is used if $x < 2$. Note that for $x = 0$, it reduces to the Langevin expression. Alternatively, the expression can be written in powers of temperature T. For example, when $x \geqslant 2$,

$$k_{\rm cap} = c_1 + c_2 T^{-1/2}, \quad (4)$$

where, $c_1 = 0.62k_L$ and $c_2 = (0.4767\mu_D/\sqrt{(2\alpha K)}k_L$. If the second term in Equation (4) is much greater than the first term, the expression has $T^{-1/2}$ dependence which is used in both the UMIST and OSU databases. We took values of polarizability and dipole moments of neutral species by following Woon & Herbst (2009). They optimized equilibrium structures at a RCCSD(T)/aug-cc-pVTZ level of theory using a finite field approach to obtain the dipole moment and dipole polarizability components. According to their calculations, values of the polarizabilities (α) for HCl, H_2O, H_2, CO, and NH_3 are 2.538, 1.406, 0.773, 1.951, and 2.087 Å^3, respectively, and values of the dipole moments (μ_D) for HCl, H_2O, H_2, CO, and NH_3 are 1.075, 1.845, 0, 0.101, and 1.519 D, respectively. The computation of polarizability and dipole moments depend on the derivatives of electronic energy with respect to the external electric field. This electronic energy is not dependent on the mass of the nuclei as calculations are based on a Born–Oppenheimer approximation. But experimental differences arise mostly from differences in vibrationally averaged structure. In our case, polarizability and dipole moments of HD, D_2, DCl, and NH_2D are assumed to be similar to their hydrogenated counter parts. Plugging these values (polarizability and dipole moment of the neutral species and reduced mass of the reactants) into the above equations, we calculated reaction rates for the ion–neutral reactions ((A2)–(A24)).

Molecular ions could be destroyed by the following DR reactions:

$$DCl^+ + e^- \rightarrow Cl + D, \quad \text{(A25)}$$

$$D_2Cl^+ + e^- \rightarrow Cl + D + D, \quad \text{(A26)}$$

$$D_2Cl^+ + e^- \rightarrow DCl + D, \quad \text{(A27)}$$

$$HDCl^+ + e^- \rightarrow Cl + D + H, \quad \text{(A28)}$$

$$HDCl^+ + e^- \rightarrow DCl + H. \quad \text{(A29)}$$

In the absence of experimentally determined rate coefficients, following Neufeld & Wolfire (2009), we use Equations (5) and (6) for the computation of DR rate coefficients ((A25)–(A29)) for diatomic and triatomic molecular ions, namely,

$$k = 2 \times 10^{-7}(T/300)^{-1/2}\ {\rm cm^3\ s^{-1}} \quad (5)$$

and

$$k = 1.2 \times 10^{-7}(T/300)^{-0.85}\ {\rm cm^3\ s^{-1}}. \quad (6)$$

Table 1
Initial Abundances Used Relative to Total Hydrogen Nuclei

Species	Abundance
H_2	5.00×10^{-01}
He	1.00×10^{-01}
N	2.14×10^{-05}
O	1.76×10^{-04}
H_3^+	1.00×10^{-11}
C^+	7.30×10^{-05}
S^+	8.00×10^{-08}
Si^+	8.00×10^{-09}
Fe^+	3.00×10^{-09}
Na^+	2.00×10^{-09}
Mg^+	7.00×10^{-09}
P^+	3.00×10^{-09}
Cl^+	4.00×10^{-09}
e^-	7.31×10^{-05}
HD	1.6×10^{-05}

Following the destruction pathways of HCl (Woodall et al. 2007), we have assumed that DCl could also be destroyed by cosmic ray-induced (CRPHOT) photo reactions:

$$\mathrm{DCl} + \mathrm{CRPHOT} \rightarrow \mathrm{Cl} + \mathrm{D}. \quad \text{(A30)}$$

The rate of cosmic ray-induced photo reaction (A30) could be adopted as follows:

$$k_{\mathrm{CR}}(T) = \alpha(T/300)^{\beta}\gamma/(1-\omega)\,\mathrm{s}^{-1}, \quad (7)$$

where the cosmic-ray ionization rate is denoted by α, photo reaction probability per cosmic ray ionization is denoted by γ, and ω denotes the reflection coefficients of dust grain in far UV. Following reaction HCl + CRPHOT → H + Cl in Woodall et al. (2007), here too we assume that $\alpha = 1.3 \times 10^{-17}$, $\beta = 0$, $\gamma = 305$, and $\omega = 0.6$.

DCl could also be dissociated by following interstellar photo reaction (PHOTON):

$$\mathrm{DCl} + \mathrm{PHOTON} \rightarrow \mathrm{Cl} + \mathrm{D}. \quad \text{(A31)}$$

The rate coefficient for reaction (A31) could be calculated by using the following relation:

$$k_{\mathrm{Phot}} = \alpha \exp(-\gamma A_V)\,\mathrm{s}^{-1}, \quad (8)$$

where A_V is the visual extinction and $\gamma = 1.8$ is used following the reaction HCl + PHOTON → Cl + H in Woodall et al. (2007).

In our model, we assume that gas and grains are coupled through accretion and thermal/cosmic-ray evaporation processes. To model the environment of the outer edge of a dense interstellar cloud or a diffuse cloud, we use $T = 10$ K, $n_{\mathrm{H}} = 10^3$–10^4 cm^{-3}, $A_V = 0.01$–10 mag. Following Roberts & Millar (2000), in Table 1, initial elemental abundances relative to the total hydrogen nuclei is shown. This type of initial abundances are often adopted for the cold dark cloud. All computed/estimated rate coefficients ((A1)–(A31)) are provided in Table 2 for $T = 10$ K, $A_V = 10$.

Table 2
Formation/Destruction of Deuterated Chloronium Ions and Related Species

Reaction	Reaction Type	Rate Coefficients
$H^+ + DCl \rightarrow DCl^+ + H$ (A1)	Charge exchange	1.1×10^{-10} cm^3 s^{-1}
$He^+ + DCl \rightarrow Cl^+ + He + D$ (A2)	Ion–neutral	1.8×10^{-8} cm^3 s^{-1}
$C^+ + DCl \rightarrow CCl^+ + D$ (A3)	Ion–neutral	8.3×10^{-10} cm^3 s^{-1}
$CH_3^+ + DCl \rightarrow H_2CCl^+ + HD$ (A4)	Ion–neutral	7.7×10^{-09} cm^3 s^{-1}
$NH_2D^+CCl^+ \rightarrow HCNH^+ + DCl$ (A5)	Ion–neutral	9.5×10^{-09} cm^3 s^{-1}
$H_2O + HDCl^+ \rightarrow DCl + H_3O^+$ (A6)	Ion–neutral	1.2×10^{-08} cm^3 s^{-1}
$CO + HDCl^+ \rightarrow DCl^+HCO^+$ (A7)	Ion–neutral	2.5×10^{-10} cm^3 s^{-1}
$H_2 + DCl^+ \rightarrow HDCl^+ + H$ (A8)	Ion–neutral	1.5×10^{-09} cm^3 s^{-1}
$H_3^+ + DCl \rightarrow HDCl^+ + H_2$ (A9)	Ion–neutral	1.5×10^{-08} cm^3 s^{-1}
$CH_5^+ + DCl \rightarrow HDCl^+ + CH_4$ (A10)	Ion–neutral	7.3×10^{-09} cm^3 s^{-1}
$HD + DCl^+ \rightarrow D_2Cl^+ + H$ (A11)	Ion–neutral	1.2×10^{-09} cm^3 s^{-1}
$H_2D^+ + DCl \rightarrow D_2Cl^+ + H_2$ (A12)	Ion–neutral	1.3×10^{-08} cm^3 s^{-1}
$HD_2^+ + DCl \rightarrow D_2Cl^+ + HD$ (A13)	Ion–neutral	1.2×10^{-08} cm^3 s^{-1}
$CH_4D^+ + DCl \rightarrow D_2Cl^+ + CH_4$ (A14)	Ion–neutral	7.2×10^{-09} cm^3 s^{-1}
$H_2O + D_2Cl^+ \rightarrow DCl + H_2DO^+$ (A15)	Ion–neutral	1.2×10^{-08} cm^3 s^{-1}
$CO + D_2Cl^+ \rightarrow DCl + DCO^+$ (A16)	Ion–neutral	2.5×10^{-10} cm^3 s^{-1}
$HD + Cl^+ \rightarrow DCl^+ + H$ (A17)	Ion–neutral	1.2×10^{-09} cm^3 s^{-1}
$D_2 + Cl^+ \rightarrow DCl^+ + D$ (A18)	Ion–neutral	1.1×10^{-09} cm^3 s^{-1}
$H_2 + DCl^+ \rightarrow HDCl^+ + H$ (A19)	Ion–neutral	1.5×10^{-09} cm^3 s^{-1}
$HD + HCl^+ \rightarrow HDCl^+ + H$ (A20)	Ion–neutral	1.2×10^{-09} cm^3 s^{-1}
$D_2 + HCl^+ \rightarrow HDCl^+ + D$ (A21)	Ion–neutral	1.1×10^{-09} cm^3 s^{-1}
$H_2D^+ + Cl \rightarrow DCl^+ + H_2$ (A22)	Ion–neutral	1.0×10^{-09} cm^3 s^{-1}
$HD_2^+ + Cl \rightarrow DCl^+ + HD$ (A23)	Ion–neutral	1.0×10^{-09} cm^3 s^{-1}
$D_3^+ + Cl \rightarrow DCl^+ + D_2$ (A24)	Ion–neutral	1.0×10^{-09} cm^3 s^{-1}
$DCl^+ + e^- \rightarrow Cl + D$ (A25)	Dissociative recombination	6.0×10^{-6} s^{-1}
$D_2Cl^+ + e^- \rightarrow Cl + D + D$ (A26)	Dissociative recombination	1.2×10^{-5} s^{-1}
$D_2Cl^+ + e^- \rightarrow DCl + D$ (A27)	Dissociative recombination	1.2×10^{-5} s^{-1}
$HDCl^+ + e^- \rightarrow Cl + D + H$ (A28)	Dissociative recombination	1.2×10^{-5} s^{-1}
$HDCl^+ + e^- \rightarrow DCl + H$ (A29)	Dissociative recombination	1.2×10^{-5} s^{-1}
DCl + CRPHOT → Cl + D (A30)	Cosmic ray-induced photodissociation	9.9×10^{-15} s^{-1}
DCl + PHOTON → Cl + D (A31)	Photodissociation	1.7×10^{-17} s^{-1}

Table 3
Theoretical and Experimental Quadrupole Coupling Constants of Chlorine in H_2Cl^+, D_2Cl^+, and $HDCl^+$

Species	Constants	Theoretical Values in MHz[a]	Experimental Values
H_2Cl^+	χ_{aa}	−51.8851	−53.44
	χ_{bb}	−14.3463	−15.71
	χ_{cc}	66.2314	69.15
	χ_{ab}	−0.4689	...
$HDCl^+$	χ_{aa}	−39.2014	...
	χ_{bb}	−27.1076	...
	χ_{cc}	66.3090	...
	χ_{ab}	17.4213	...
D_2Cl^+	χ_{aa}	−51.8863	...
	χ_{bb}	−14.3470	...
	χ_{cc}	66.2333	...
	χ_{ab}	−0.3328	...

Note. [a] Saito & Yamamoto (1988).

3. RESULTS AND DISCUSSION

3.1. Chemical Properties

Interstellar chloronium (H_2Cl^+) is an asymmetric top with C_{2V} symmetry. We performed quantum chemical simulation (MP2/aug-cc-pVQZ level of theory) for geometry optimization and energy calculation of a chloronium ion. Ground-state energies of H_2Cl^+ in gas and ice phases are found to be −460.55382 AU and −460.67002 AU (1 atomic unit = 27.21 eV), respectively. Due to solute–solvent electrostatic interaction (dipole level), ground-state energy in the ice phase is found to be lower than ground-state energy in the gas phase. The solvent effect also brings changes in geometrical parameters of these species. Our results confirm that polarization of solute by continuum has important effects on absolute and relative solvation energies, which in turn change the energy of the respective species. The ground-state energy of D_2Cl^+ and $HDCl^+$ are found to be similar to the ground-state energy of H_2Cl^+ in gas and ice phases. This is due to the fact that ground-state energy and structure calculations are made by using the Born–Oppenheimer approximation so isotopic mass is not a factor in the Hamiltonian. The dipole moment of chloronium in gas and ice phases are found to be 1.98 and 2.2024 D, respectively. The dipole moment of chloronium has been estimated as 1.89 D in ab initio calculations performed by H. S. P. Müller (2008, unpublished)[3]. According to Puzzarini et al. (2010), additional splitting in a rotational spectrum is governed by nuclear quadrupole coupling of molecules. Moreover, according to them, quantum chemical calculations could be extremely helpful for fine structure analysis because it could provide an electric-field gradient at corresponding nuclei. In Table 3, we show a comparison of experiment and theoretical ground-state quadrupole coupling constants of chlorine H_2Cl^+ for a Mp2/aug-cc-pVQZ level of theory. Also, for the first time, we provide quadrupole coupling constants of chlorine in D_2Cl^+ and $HDCl^+$ in the same table.

3.2. Chemical Evolution and Deuterium Enrichment

In Figure 1, the chemical evolution of the chloronium ion and related species are shown. To mimic the interstellar scenario, we consider $n_H = 10^4$ cm^{-3}, $A_V = 10$, and $T = 10$ K. It is initially assumed that all deuteriums are locked in the form of HD. Initial abundances of HD and H_2 are taken to be 1.6×10^{-5} and 0.5, respectively (Table 1), with respect to total number of hydrogen nuclei. This implies an initial fractionation ratio of 3.2×10^{-5}. Unless otherwise stated, we use this initial fractionation ratio in all of our simulations. In our gas–grain model, we assume that all of the neutral species could be depleted to icy grain with a sticking coefficient of unity. Depleted species are allowed to populate the gas phase via thermal evaporation and cosmic-ray evaporation processes. Due to depletion of neutral species, the rate of production of their relative ions are decreased. DR processes then lead to the destruction of these ionic species. As a result, abundances of these ions are decreased. In our simulation, we evolved our chemical code to a time comparable to the lifetime of a generic molecular cloud ($\sim 10^7$ yr). From Figure 1, it is clear that most of the species attain peak values near $\sim 10^5$ yr. In the literature, a number of theoretical models attempted to find time variation of physical properties of protostars since the beginning of gravitational collapse (Smith 1998; Myers et al. 1998). The time sequence of evolutionary stages determined by various models are more or less similar but their estimates of absolute ages vary significantly (Emprechtinger et al. 2008). According to Froebrich et al. (2005), the absolute age for Class 0/I borderline objects, for example, varies between 10^4 and a few times 10^5 yr. Our simulation results in Figure 1 show that within this time frame, some species will attain peak values. It is also evident that one of the isotopomers of H_2Cl^+ (i.e., $HDCl^+$ from Figure 1) is reasonably abundant within this time frame of collapse. So it is expected to be observed with ALMA, for example.

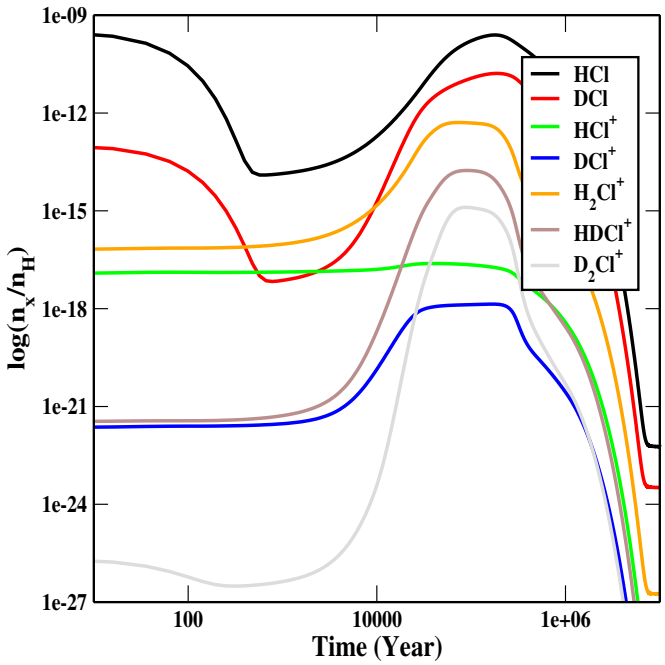

Figure 1. Time evolution of the chloronium ion and its related species. (A color version of this figure is available in the online journal.)

Following Shalabiea & Greenberg (1994) and Das & Chakrabarti (2011), the column density of a species could be calculated using the following relation:

$$N(A) = n_H x_i R, \quad (9)$$

where, n_H is the total hydrogen number density, x_i is the abundance of the ith species, and R is the path length along

[3] See also http://www.astro.uni-koeln.de/cgi-bin/cdmsinfo?file=e037504.cat

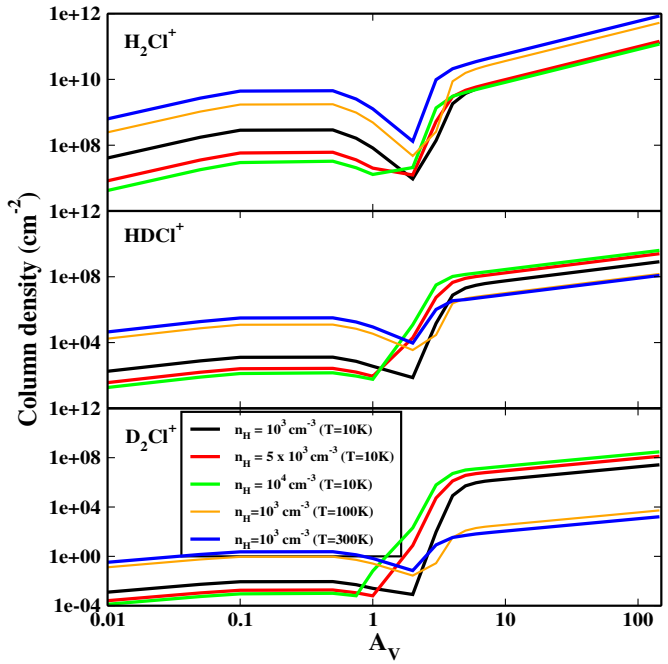

Figure 2. Variation of peak column densities with visual extinction parameter (A_V).
(A color version of this figure is available in the online journal.)

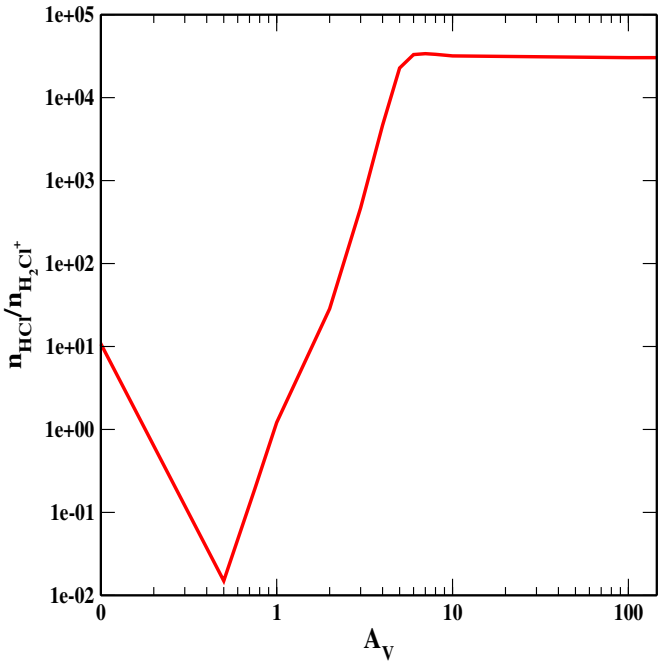

Figure 3. Variation of HCl/H_2Cl^+ column density ratio with A_V.
(A color version of this figure is available in the online journal.)

the line of sight (=$(1.6 \times 10^{21} \times A_V)/n_H$). According to Lis et al. (2010), H_2Cl^+ is predicted to be the most abundant in those environments where ultraviolet radiation is strong (i.e., in diffuse clouds, or near surfaces of dense clouds that are illuminated by nearby O and B stars). In Figure 2, we mimic these features by varying the visual extinction parameter (A_V) from 0.1 to 145. This high value of visual extinction ($A_V = 145$) could be used for W33A (Allamandola et al. 1992). Variation of peak column densities of the chloronium ion and its isotopomers are shown for different number density clouds (10^3–10^4 cm^{-3}). Abundance of H_2Cl^+ roughly remains constant beyond $A_V = 5$. From Equation (9), it is clear that the column density is directly proportional to A_V. As the abundance (x_i) remains constant beyond $A_V = 5$, peak column densities increase linearly. For $A_V < 4$, peak column densities are heavily affected. Column densities are at their maximum around heavily shielded regions ($A_V > 4$). Lis et al. (2010) computed the column density of H_2Cl^+ to be 2.2–3.4 $\times$ 10^{13} cm^{-2} along NGC 6334I by assuming a 5 K excitation temperature. Neufeld & Wolfire (2009) identified H_2Cl^+ around photodissociation regions. According to their prediction, column density of H_2Cl^+ around a photodissociation region ($n_H \sim 10^4$ cm^{-3}, $\kappa_{UV} \sim 10^4$) would be $\sim$2.6 $\times$ 10^{11} cm^{-2}. κ_{UV} is the UV radiation field which is normalized with respect to the mean interstellar value by Draine (1978). Neufeld & Wolfire (2009) also predicted column density of chloronium $\sim 3 \times 10^{11}$ cm^{-2} for the conditions which could be applicable to the environment of the Orion Bar photon-dominated region (PDR) ($n_H \sim 6 \times 10^4$ cm^{-3} and $\kappa_{UV} \sim 3 \times 10^4$). Their predicted column density was also 100 times smaller than what is found in recent observations by Lis et al. (2010). Neufeld et al. (2012) mentioned that this theoretically predicted value should not be compared directly with the observed values because theoretical prediction was for the perpendicular column density whereas the Orion Bar PDR was observed nearly edge-on. They expect that geometrical enhancement in the observed value of the column density by a factor of four could be possible. In our case, we find a peak column density of $H_2Cl^+ \sim 1.3 \times 10^{11}$ cm^{-2} in between $A_V = 0.1$–145, $n_H = 10^3$–10^4 cm^{-3}, and $T = 10$ K. We also carried out our simulation at a higher temperature to find out the effects of temperature on the formation of chloronium ion. For this case, we assumed $n_H = 10^3$ cm^{-3} and varied visual extinction (A_V) in between 0.1–145for temperature 100 K and 300 K, respectively (Figure 2). From Figure 2, it is evident that column density of the chloronium ion increases with temperature, and we have the maximum column density of 8.49 $\times$ 10^{11} cm^{-2} at 300 K. Column densities of deuterated forms of the chloronium ion are also heavily affected by an increase in temperature. For $A_V < 2$, column densities of these deuterated ions increases whereas for $A_V > 2$, they are found to decrease when compared to the $T = 10$ K case.

Lis et al. (2010) derived HCl/H_2Cl^+ column density ratios to be in the range $\sim$1–10, for diffuse and dense PDRs. In Figure 3, we show the variation of HCl/H_2Cl^+ column density ratio with A_V. For $A_V < 2$ (i.e., for the strong radiation field), our results are in line with observations. For this case, we assumed $n_H = 10^4$ cm^{-3}, $T = 10$ K, and HCl/H_2Cl^+ column density ratio was taken after the simulation time scale of $\sim 10^7$ yr.

In Figure 4, we show variation of the fractionation ratio of HCl, HCl^+, and H_2Cl^+ with an initial n_{HD/H_2} ratio. For this case, we assumed $n_H = 10^4$ cm^{-3}, $A_V = 10$, and $T = 10$ K. HCl and HCl^+ are found to be heavily fractionated, always crossing elemental D/H ratio ($\sim 10^{-5}$; Linsky et al. 1995). It is interesting to note that in our simulations, the $HDCl^+/H_2Cl^+$ column density ratio is always above the elemental D/H ratio. The fractionation ratio of D_2Cl^+ molecule crossing the elemental D/H ratio beyond initial n_{HD/H_2} ratio 10^{-6}. As the H_2Cl^+ molecule is heavily fractionated, we strongly suggest to look for $HDCl^+$ molecules in the same molecular clouds where the H_2Cl^+ molecule was already been observed.

Table 4
Vibrational Frequencies of Different Forms of Chloronium in Gas Phase, in Water Ice, and in Mixed Ice at the MP2/aug-cc-pVQZ Level of Theory

Species	Charge	Spin State	Peak Positions (Gas Phase) (Wavenumber) (in cm^{-1})	Absorbance	Peak Positions (H_2O Ice) (Wavenumber) (in cm^{-1})	Absorbance	Peak Positions (Mixed Ice) (Wavenumber) (in cm^{-1})	Absorbance
H_2Cl^+	Cation	Singlet	1213.01	23.5567	1208.84	25.3066	1209.44	24.9379
			2779.83	342.2380	2822.06	409.2761	2818.33	403.9254
			2789.60	213.5581	2834.00	267.9801	2831.03	262.6758
D_2Cl^+	Cation	Singlet	870.12	8.0653	866.89	8.8043	867.34	8.6495
			1995.63	164.4252	2025.45	198.2665	2022.82	195.5651
			1998.19	100.4653	2030.55	127.2815	2028.39	124.6488
$HDCl^+$	Cation	Singlet	1055.58	21.0134	1051.30	23.6298	1051.20	23.2953
			1996.92	132.2521	2027.98	163.0641	2025.58	160.4419
			2784.69	278.3963	2828.05	338.3961	2824.70	333.0264

Table 5
Theoretical and Available Experimental Rotational Parameters of Chloronium and Its Different Isotopomers at MP2/aug-cc-pVQZ Level of Theory

Species	Rotational Constants	Values in MHz	Experimental Values in MHz[a]	Distortional Constants	Values in MHz	Experimental Values in MHz[a]
H_2Cl^+ in gas phase	A	336730.77093	337353.229	D_J	0.19899×10^2	...
	B	274941.86042	273586.425	D_{JK}	-0.73569×10^2	−71.814
	C	151335.22094	148100.004	D_K	0.12577×10^3	...
				d_1	-0.83773×10^1	...
				d_2	0.58014	...
$HDCl^+$ in gas phase	A	309898.96477		D_J	0.35636×10^1	
	B	153561.70202		D_{JK}	-0.92932×10^1	
	C	102697.60073		D_K	0.98535×10^2	
				d_1	-0.13938×10^1	
				d_2	−0.11650	
D_2Cl^+ in gas phase	A	177672.18281		D_J	0.48691×10^1	
	B	137566.23157		D_{JK}	-0.17934×10^2	
	C	77526.70474		D_K	0.33137×10^2	
				d_1	-0.20906×10^1	
				d_2	-0.81717×10^{-1}	

Note. [a] Saito & Yamamoto (1988).

3.3. Spectral Analysis

We now turn to spectral properties of H_2Cl^+ and two of its isotopomers. For vibrational spectra, we compute infrared peak positions with their absorbance in gas phase as well as in water ice and mixed ice phases. In Table 4, we present these for H_2Cl^+ and two of its isotopomers, namely, D_2Cl^+ and $HDCl^+$. We find that the most intense mode of H_2Cl^+ in the gas phase appears nearly at 2779.83 cm^{-1}. This peak is shifted in the ice phase (water ice) by nearly 42 cm^{-1} and appears at 2822.06 cm^{-1}. The second strongest peak in the gas phase appears at 2789.60 cm^{-1}. It is also shifted in the ice phase. To have a more realistic condition, instead of only the water ice, we have considered a mixed ice mantle, which contains 70% water, 20% methanol, and 10% CO_2 molecules (Keane et al. 2001; Das & Chakrabarti 2011; Majumdar et al. 2013a, 2013b; Das et al. 2013b). The Gaussian 09W program uses a dielectric constant of water to be ∼78.5. For the case of mixed ice, we put the dielectric constant of the medium to be 61, which is calculated by taking an weighted average of the dielectric constants of H_2O, CH_3OH, and CO_2. We note that the most intense peak in gas phase is shifted in mixed ice also (Table 4). Isotope effects on chemical shifts is caused by differences in vibrational modes due to different isotope masses. Each of the H_2Cl^+, D_2Cl^+, and $HDCl^+$ molecules has a unique spectrum because substitution of isotope changes reduced mass of corresponding molecule. We find that the most intense mode of D_2Cl^+ in gas phase appears at 1995.63 cm^{-1}. This peak is shifted in ice phase by 29.82 cm^{-1}, i.e., at 2025.45 cm^{-1}. The second strongest peak in gas phase which appears at 1998.19 cm^{-1} is also shifted in ice phase and appears at 2030.55 cm^{-1}. The most intense peak in gas phase is similarly shifted in mixed solvated grain. Infrared peak positions with their absorbance in gas phase as well as in ice and mixed ice phases are marked for D_2Cl^+ and $HDCl^+$ in Table 4. In Figures 5 and 6, we show how the isotopic substitution (D_2Cl^+ and $HDCl^+$) plays a part in vibrational progressions of H_2Cl^+ in both gas phase and ice phase. Our results clearly show differences between spectroscopic parameters computed for the interstellar chloronium ion in gas phase and ice phase. These differences can be explained due to electrostatic effects that are often much less important for species placed in a solvent with high dielectric constant than they are in gas phase (Foresman & Frisch 1996).

In Table 5, we summarize our calculated theoretical values of rotational and quartic centrifugal distortion constants for H_2Cl^+, D_2Cl^+, and $HDCl^+$ in gas phase. Calculated constants are corrected for each vibrational state as well as vibrationally

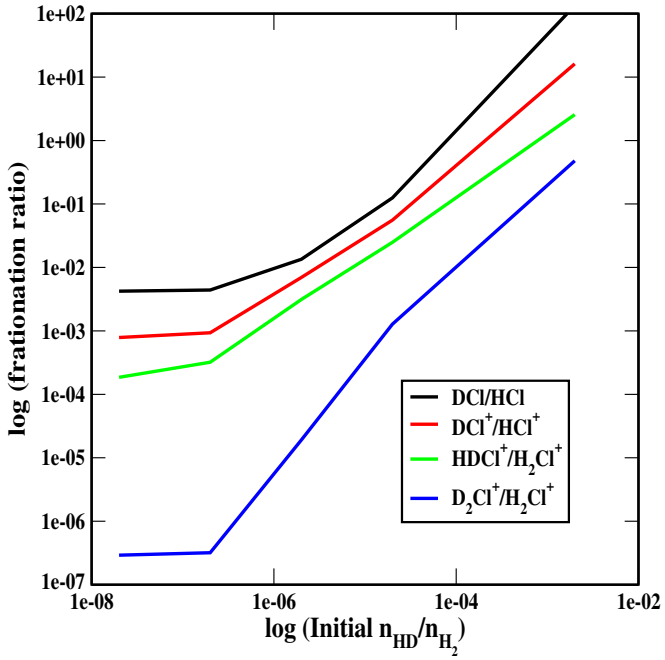

Figure 4. Variation of fractionation ratio with an initial HD/H_2 ratio.
(A color version of this figure is available in the online journal.)

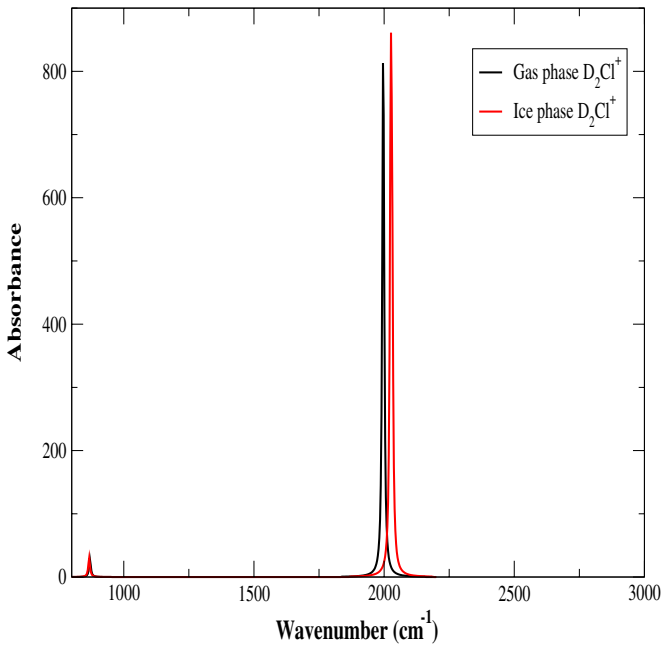

Figure 5. Infrared spectrum of D_2Cl^+ in gas as well as in ice phase.
(A color version of this figure is available in the online journal.)

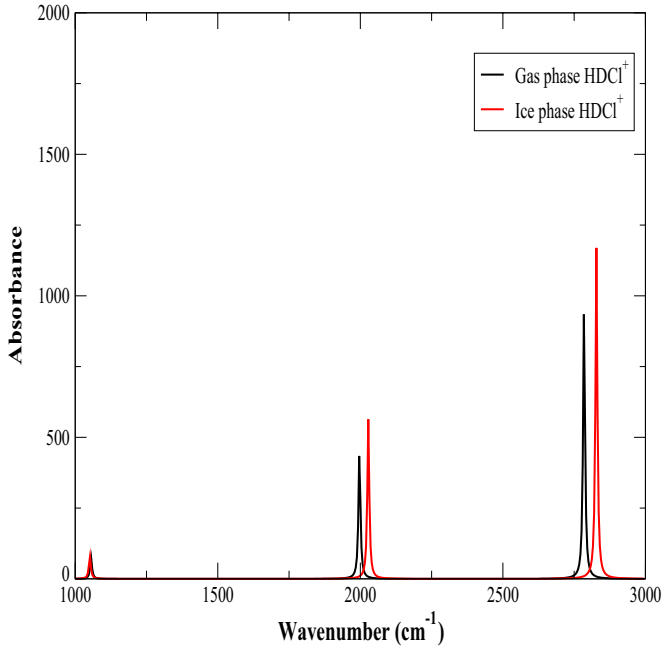

Figure 6. Infrared spectrum of $HDCl^+$ in gas as well as in ice phase.
(A color version of this figure is available in the online journal.)

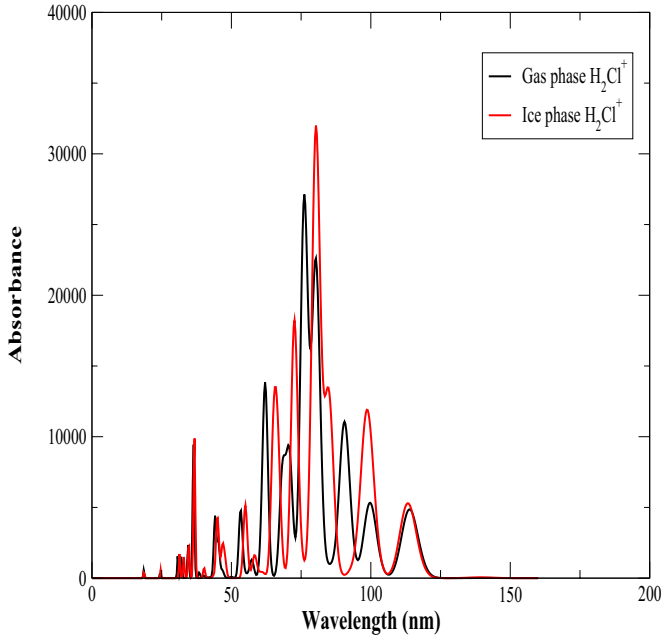

Figure 7. Electronic absorption spectrum of H_2Cl^+ in gas phase and in ice phase.
(A color version of this figure is available in the online journal.)

averaged structures. The MP2/aug-cc-pVQZ level of theory has been used to perform these calculations for gas phase H_2Cl^+, D_2Cl^+, and $HDCl^+$. We compare our calculated spectroscopic constants (A, B, C, D_{JK}) of H_2Cl^+ with Saito & Yamamoto (1988) in Table 5. In order to summarize the outcome of our calculations about rotational spectroscopy, we prepare our spectral information for one of the isotopologues of H_2Cl^+ ($HDCl^+$) as per guidelines of JPL (Table 7 of the Appendix). Computed transitions are falling in between the 3 and 9 bands of ALMA (84–720 GHz). Our computed column density also suggests that it could also be observed around the similar region, where H_2Cl^+ was observed.

Different electronic absorption spectral parameters of H_2Cl^+ in gas phase are given in Table 6. In gas phase, the spectrum is characterized by five intense peaks at wavelengths of 90.6, 80.3, 76.1, 62.3, and 36.4 nm (Figure 7). These intense peaks are assigned due to HOMO–LUMO transitions. These transitions correspond to H–0 → L+2, H–2 → L+0, H–1 → L+3, H–2 → L+2, and H–0 → L+13. Depending on the composition of interstellar grain mantle, peak positions in ice phase are shifted. These features are presented in Table 6 with corresponding transition details. Figure 7 clearly shows some differences in gas and ice phase electronic absorption spectra of H_2Cl^+.

Table 6
Electronic Transitions of H_2Cl^+ at B3LYP/6-311++G** Level of Theory

Species	Wavelength in nm	Absorbance	Oscillator Strength	Transitions	Contribution in %
	113.9	4864.07	0.1201	H–1 → L+0	98
	99.7	5322.96	0.1316	H–1 → L+1	90
	90.6	11062.41	0.2728	H–0 → L+2	100
	80.3	22614.49	0.5051	H–2 → L+0	66
	76.1	27125.91	0.4172	H–1 → L+3	70
	70.8	9307.55	0.211	H–2 → L+1	57
H_2Cl^+ in gas phase	62.3	13154.01	0.2709	H–2 → L+2	90
	57.3	1301.54	0.03	H–0 → L+9	100
	53.3	4644.87	0.1117	H–1 → L+8	96
	44.2	4413.36	0.1047	H–2 → L+9	90
	36.4	9444.575	0.2395	H–0 → L+13	100
	34.5	2347.95	0.0594	H–1 → L+13	98
	32.09	1508.80	0.0205	H–3 → L+10	100
	30.79	1549.00	0.0402	H–3 → L+10	100
	113.3	5297.52	0.1308	H–1 → L+0	98
	98.1	11706.04	0.513	H–0 → L+2	97
	80.3	31995.46	0.7694	H–2 → L+0	66
	72.6	18217.29	0.4457	H–2 → L+1	83
	65.1	13505.80	0	H–2 → L+4	74
	58.4	1618.54	0.0381	H–0 → L+9	100
H_2Cl^+ in ice phase	55.0	4755.99	0.1215	H–1 → L+8	96
	46.8	2349.30	0.0526	H–2 → L+8	91
	45.2	4262.98	0	H–2 → L+11	100
	40.21	697.86	0.018	H–2 → L+12	48
	36.7	9872.20	0.2521	H–0 → L+13	100
	34.7	2272.75	0.065	H–1 → L+13	99
	32.9	1495.5532	0.0207	H–3→L+11	100
	31.4	1707.95	0.0437	H–3→L+12	82
	113.5	5344.97	0.1321	H–1 → L+0	98
	99.4	206.40	0.1575	H–1 → L+1	92
	80.3	31849.63	0.7566	H–2 → L+0	63
H_2Cl^+ in mixed ice	72.6	18544.85	0.4527	H–2 → L+1	82
	65.7	13565.30	0	H–2 → L+5	100
	58.4	1616.83	0.0388	H–0 → L+9	100
	54.9	4785.04	0.1193	H–1 → L+8	96
	36.7	9833.04	0.2511	H–0 → L+13	100

4. CONCLUSIONS

Protonated hydrogen chloride or chloronium (H_2Cl^+) ion has been recently identified toward Sgr A, W31C. In this paper, we investigated the existence and different aspects of its two isotopomers, namely, $HDCl^+$ and D_2Cl^+. The major results of this paper are as follows.

1. Langevin theory and parameterized trajectory theory are used for the computation of various ion–molecular reaction rates containing H_2Cl^+ and its related species.
2. Our chemical modeling shows that $HDCl^+$ could be efficiently formed in the gas phase and the emission line should be strong enough to be observed.
3. We explored vibrational, rotational, and electronic spectral properties of H_2Cl^+, D_2Cl^+, and $HDCl^+$ in different astrophysical environments. The resulting chemical parameters could assist observers in identifying these molecules around an interstellar molecular cloud. In the Appendix, we present a representative catalog file in JPL format for gas phase $HDCl^+$, which will be useful for observational purposes.

A.D. is grateful to ISRO for financial support through a respond project (Grant No. ISRO/RES/2/372/11-12), S.K.C. is grateful for a DST project (Grant No.SR/S2/HEP-40/2008), and L.M. thanks MOES for partial funding during this work. The authors would like to thank the anonymous referee whose valuable suggestions have helped to improve this paper significantly.

APPENDIX

The existence of an interstellar chloronium ion has recently been reported by *Herschel Space Observatory*'s HIFI (Neufeld et al. 2012). Our calculations show that one of the deuterated forms of the chloronium ion ($HDCl^+$) is significantly abundant and should be observed. In order to summarize results of our computation on rotational spectroscopy, we prepare our spectral information for $HDCl^+$ (Table 7 in the format of a JPL catalog) to assist its detection around the ISM. In Table 7, the computed rotational transitions for the gas phase $HDCl^+$ is shown. This table is prepared with our calculated values of spectroscopic constants which are given in Table 5. In Table 7, we have given the rotational transitions in MHz units. The corresponding intensity of lines are tabulated in nm^2 MHz units. The intensity of any line represents an absorption cross section over spectral line shape (calculated at 300 K and tabulated in base 10 logarithm units). Other parameters that are responsible for the computation of line frequencies are given in the footnote of Table 7.

Table 7
Different Rotational Transitions and Its Related Parameters for Gas Phase $HDCl^+$ in the Format of the JPL Catalog

Frequency[a]	Uncertainty[b]	I[c]	D[d]	E_{lower}[e]	g_{up}[f]	Tag[g]	QnF[h]	Qn_{up}[i]	Qn_{lower}[j]
257376.1993	0.0000	−2.8248	3	−0.0000	4	38001	335	1 0 1 2 2	0 0 0 2 1
257376.1993	0.0000	−2.4316	3	−0.0000	4	38001	335	1 0 1 2 2	0 0 0 2 2
257376.1993	0.0000	−2.8248	3	−0.0000	4	38001	335	1 0 1 2 2	0 0 0 2 1
257376.1993	0.0000	−2.7830	3	−0.0000	4	38001	335	1 0 1 2 2	0 0 0 2 3
257376.2326	0.0000	−2.7797	3	−0.0000	6	38001	335	1 0 1 2 3	0 0 0 2 2
257376.2326	0.0000	−2.0650	3	−0.0000	6	38001	335	1 0 1 2 3	0 0 0 2 3
257376.2592	0.0000	−2.7200	3	−0.0000	2	38001	335	1 0 1 2 1	0 0 0 2 1
257376.2592	0.0000	−2.8187	3	−0.0000	2	38001	335	1 0 1 2 1	0 0 0 2 2
257386.0031	0.0000	−2.2865	3	−0.0000	4	38001	335	1 0 1 3 2	0 0 0 2 1
257386.0031	0.0000	−2.7946	3	−0.0000	4	38001	335	1 0 1 3 2	0 0 0 2 2
257386.0031	0.0000	−4.1421	3	−0.0000	4	38001	335	1 0 1 3 2	0 0 0 2 3
257386.0181	0.0000	−1.8634	3	−0.0000	8	38001	335	1 0 1 3 4	0 0 0 2 3
257386.0529	0.0000	−2.0650	3	−0.0000	6	38001	335	1 0 1 3 3	0 0 0 2 2
257386.0529	0.0000	−2.7796	3	−0.0000	6	38001	335	1 0 1 3 3	0 0 0 2 3
257393.8667	0.0000	−2.8187	3	−0.0000	2	38001	335	1 0 1 1 1	0 0 0 2 1
257393.8667	0.0000	−2.7199	3	−0.0000	2	38001	335	1 0 1 1 1	0 0 0 2 2
257393.8669	0.0000	−3.7450	3	−0.0000	4	38001	335	1 0 1 1 2	0 0 0 2 1
257393.8669	0.0000	−2.2901	3	−0.0000	4	38001	335	1 0 1 1 2	0 0 0 2 3
257393.8670	0.0000	−2.8123	3	−0.0000	4	38001	335	1 0 1 1 2	0 0 0 2 2
514659.8572	0.0000	−6.7938	3	8.5857	4	38001	335	2 0 2 3 2	1 0 1 1 1
514659.8824	0.0000	−7.4094	3	8.5857	6	38001	335	2 0 2 3 3	1 0 1 1 2
514666.8692	0.0000	−3.1365	3	8.5857	2	38001	335	2 0 2 2 1	1 0 1 1 2
514666.8694	0.0000	−1.7143	3	8.5857	6	38001	335	2 0 2 2 3	1 0 1 1 2
514666.8695	0.0000	−2.2435	3	8.5857	2	38001	335	2 0 2 2 1	1 0 1 1 1
514666.8696	0.0000	−2.2437	3	8.5857	4	38001	335	2 0 2 2 2	1 0 1 1 2
514666.8698	0.0000	−2.1448	3	8.5857	4	38001	335	2 0 2 2 2	1 0 1 1 1
514667.6710	0.0000	−2.8243	3	8.5855	4	38001	335	2 0 2 3 2	1 0 1 3 3
514667.6788	0.0000	−2.8208	3	8.5855	8	38001	335	2 0 2 3 4	1 0 1 3 3
514667.6964	0.0000	−1.9589	3	8.5855	6	38001	335	2 0 2 3 3	1 0 1 3 3
514667.7136	0.0000	−1.7698	3	8.5855	8	38001	335	2 0 2 3 4	1 0 1 3 4
514667.7208	0.0000	−2.1126	3	8.5855	4	38001	335	2 0 2 3 2	1 0 1 3 2
514667.7313	0.0000	−2.8220	3	8.5855	6	38001	335	2 0 2 3 3	1 0 1 3 4
514667.7463	0.0000	−2.8260	3	8.5855	6	38001	335	2 0 2 3 3	1 0 1 3 2
514669.6441	0.0000	−5.4590	3	8.5857	6	38001	335	2 0 2 4 3	1 0 1 1 2
514674.6834	0.0000	−3.6631	3	8.5855	6	38001	335	2 0 2 2 3	1 0 1 3 3
514674.6836	0.0000	−2.8877	3	8.5855	4	38001	335	2 0 2 2 2	1 0 1 3 3
514674.7183	0.0000	−2.6833	3	8.5855	6	38001	335	2 0 2 2 3	1 0 1 3 4
514674.7331	0.0000	−3.1158	3	8.5855	2	38001	335	2 0 2 2 1	1 0 1 3 2
514674.7332	0.0000	−4.5605	3	8.5855	6	38001	335	2 0 2 2 3	1 0 1 3 2
514674.7334	0.0000	−3.5845	3	8.5855	4	38001	335	2 0 2 2 2	1 0 1 3 2
514676.6697	0.0000	−1.8438	3	8.5857	4	38001	335	2 0 2 1 2	1 0 1 1 2
514676.6698	0.0000	−1.9425	3	8.5857	2	38001	335	2 0 2 1 1	1 0 1 1 2
514676.6699	0.0000	−1.9425	3	8.5857	4	38001	335	2 0 2 1 2	1 0 1 1 1
514676.6700	0.0000	−2.8364	3	8.5857	2	38001	335	2 0 2 1 1	1 0 1 1 1
514677.4582	0.0000	−2.3000	3	8.5855	6	38001	335	2 0 2 4 3	1 0 1 3 3
514677.4648	0.0000	−1.7918	3	8.5851	4	38001	335	2 0 2 3 2	1 0 1 2 1
514677.4913	0.0000	−3.6483	3	8.5851	4	38001	335	2 0 2 3 2	1 0 1 2 3
514677.4930	0.0000	−4.0096	3	8.5855	6	38001	335	2 0 2 4 3	1 0 1 3 4
514677.4991	0.0000	−1.3636	3	8.5851	8	38001	335	2 0 2 3 4	1 0 1 2 3
514677.5064	0.0000	−1.1122	3	8.5855	10	38001	335	2 0 2 4 5	1 0 1 3 4
514677.5080	0.0000	−1.3848	3	8.5855	6	38001	335	2 0 2 4 3	1 0 1 3 2
514677.5167	0.0000	−2.2922	3	8.5851	6	38001	335	2 0 2 3 3	1 0 1 2 3
514677.5172	0.0000	−1.2463	3	8.5855	8	38001	335	2 0 2 4 4	1 0 1 3 3
514677.5246	0.0000	−2.2754	3	8.5851	4	38001	335	2 0 2 3 2	1 0 1 2 2
514677.5500	0.0000	−1.5647	3	8.5851	6	38001	335	2 0 2 3 3	1 0 1 2 2
514677.5521	0.0000	−2.2942	3	8.5855	8	38001	335	2 0 2 4 4	1 0 1 3 4
514684.4770	0.0000	−2.3423	3	8.5851	2	38001	335	2 0 2 2 1	1 0 1 2 1
514684.4773	0.0000	−2.4262	3	8.5851	4	38001	335	2 0 2 2 2	1 0 1 2 1
514684.4837	0.0000	−7.6805	3	8.5855	4	38001	335	2 0 2 1 2	1 0 1 3 3
514684.5037	0.0000	−1.6815	3	8.5851	6	38001	335	2 0 2 2 3	1 0 1 2 3
514684.5039	0.0000	−2.4062	3	8.5851	4	38001	335	2 0 2 2 2	1 0 1 2 3
514684.5335	0.0000	−6.3471	3	8.5855	4	38001	335	2 0 2 1 2	1 0 1 3 2
514684.5337	0.0000	−7.0346	3	8.5855	2	38001	335	2 0 2 1 1	1 0 1 3 2
514684.5368	0.0000	−2.4322	3	8.5851	2	38001	335	2 0 2 2 1	1 0 1 2 2
514684.5370	0.0000	−2.4096	3	8.5851	6	38001	335	2 0 2 2 3	1 0 1 2 2
514684.5372	0.0000	−2.0557	3	8.5851	4	38001	335	2 0 2 2 2	1 0 1 2 2

Table 7
(Continued)

Frequency[a]	Uncertainty[b]	I[c]	D[d]	E_{lower}[e]	g_{up}[f]	Tag[g]	QnF[h]	Qn_{up}[i]	Qn_{lower}[j]
514687.2785	0.0000	−5.8721	3	8.5851	6	38001	335	2 0 2 4 3	1 0 1 2 3
514687.3117	0.0000	−6.2690	3	8.5851	6	38001	335	2 0 2 4 3	1 0 1 2 2
514687.3375	0.0000	−7.5999	3	8.5851	8	38001	335	2 0 2 4 4	1 0 1 2 3
514694.2775	0.0000	−3.8539	3	8.5851	4	38001	335	2 0 2 1 2	1 0 1 2 1
514694.2776	0.0000	−2.9352	3	8.5851	2	38001	335	2 0 2 1 1	1 0 1 2 1
514694.3040	0.0000	−2.4123	3	8.5851	4	38001	335	2 0 2 1 2	1 0 1 2 3
514694.3373	0.0000	−2.9434	3	8.5851	4	38001	335	2 0 2 1 2	1 0 1 2 2
514694.3374	0.0000	−2.8496	3	8.5851	2	38001	335	2 0 2 1 1	1 0 1 2 2
771769.9945	0.0000	−7.6046	3	25.7535	6	38001	335	3 0 3 4 3	2 0 2 1 2
771774.5695	0.0000	−6.9643	3	25.7535	4	38001	335	3 0 3 3 2	2 0 2 1 1
771774.5696	0.0000	−6.7153	3	25.7535	4	38001	335	3 0 3 3 2	2 0 2 1 2
771776.9609	0.0000	−2.9249	3	25.7533	6	38001	335	3 0 3 4 3	2 0 2 4 4
771776.9716	0.0000	−2.9289	3	25.7533	10	38001	335	3 0 3 4 5	2 0 2 4 4
771777.0070	0.0000	−1.7710	3	25.7533	8	38001	335	3 0 3 4 4	2 0 2 4 4
771777.0173	0.0000	−1.6427	3	25.7533	10	38001	335	3 0 3 4 5	2 0 2 4 5
771777.0200	0.0000	−1.8814	3	25.7533	6	38001	335	3 0 3 4 3	2 0 2 4 3
771777.0527	0.0000	−2.9291	3	25.7533	8	38001	335	3 0 3 4 4	2 0 2 4 5
771777.0661	0.0000	−2.9252	3	25.7533	8	38001	335	3 0 3 4 4	2 0 2 4 3
771779.7946	0.0000	−8.0545	3	25.7532	6	38001	335	3 0 3 4 3	2 0 2 2 2
771779.7948	0.0000	−5.5854	3	25.7532	6	38001	335	3 0 3 4 3	2 0 2 2 3
771779.8409	0.0000	−6.5020	3	25.7532	8	38001	335	3 0 3 4 4	2 0 2 2 3
771781.5480	0.0000	−4.2055	3	25.7533	8	38001	335	3 0 3 3 4	2 0 2 4 4
771781.5754	0.0000	−3.0578	3	25.7533	6	38001	335	3 0 3 3 3	2 0 2 4 4
771781.5937	0.0000	−2.9173	3	25.7533	8	38001	335	3 0 3 3 4	2 0 2 4 5
771781.5952	0.0000	−3.2034	3	25.7533	4	38001	335	3 0 3 3 2	2 0 2 4 3
771781.6070	0.0000	−7.8321	3	25.7533	8	38001	335	3 0 3 3 4	2 0 2 4 3
771781.6345	0.0000	−3.9561	3	25.7533	6	38001	335	3 0 3 3 3	2 0 2 4 3
771784.3550	0.0000	−1.6817	3	25.7535	2	38001	335	3 0 3 2 1	2 0 2 1 1
771784.3551	0.0000	−2.5820	3	25.7535	2	38001	335	3 0 3 2 1	2 0 2 1 2
771784.3698	0.0000	−1.9214	3	25.7532	4	38001	335	3 0 3 3 2	2 0 2 2 2
771784.3699	0.0000	−3.2816	3	25.7532	4	38001	335	3 0 3 3 2	2 0 2 2 3
771784.3701	0.0000	−1.4255	3	25.7532	4	38001	335	3 0 3 3 2	2 0 2 2 1
771784.3817	0.0000	−1.1519	3	25.7535	6	38001	335	3 0 3 2 3	2 0 2 1 2
771784.3818	0.0000	−0.9989	3	25.7532	8	38001	335	3 0 3 3 4	2 0 2 2 3
771784.4091	0.0000	−1.1980	3	25.7532	6	38001	335	3 0 3 3 3	2 0 2 2 2
771784.4092	0.0000	−1.9191	3	25.7532	6	38001	335	3 0 3 3 3	2 0 2 2 3
771784.4147	0.0000	−1.5815	3	25.7535	4	38001	335	3 0 3 2 2	2 0 2 1 1
771784.4149	0.0000	−1.6789	3	25.7535	4	38001	335	3 0 3 2 2	2 0 2 1 2
771786.7559	0.0000	−2.0839	3	25.7533	8	38001	335	3 0 3 5 4	2 0 2 4 4
771786.7817	0.0000	−2.0168	3	25.7529	6	38001	335	3 0 3 4 3	2 0 2 3 3
771786.7994	0.0000	−3.6919	3	25.7529	6	38001	335	3 0 3 4 3	2 0 2 3 4
771786.8016	0.0000	−3.9953	3	25.7533	8	38001	335	3 0 3 5 4	2 0 2 4 5
771786.8072	0.0000	−1.1157	3	25.7529	6	38001	335	3 0 3 4 3	2 0 2 3 2
771786.8101	0.0000	−0.8416	3	25.7529	10	38001	335	3 0 3 4 5	2 0 2 3 4
771786.8131	0.0000	−0.6956	3	25.7533	12	38001	335	3 0 3 5 6	2 0 2 4 5
771786.8150	0.0000	−0.8996	3	25.7533	8	38001	335	3 0 3 5 4	2 0 2 4 3
771786.8180	0.0000	−0.7969	3	25.7533	10	38001	335	3 0 3 5 5	2 0 2 4 4
771786.8278	0.0000	−0.9754	3	25.7529	8	38001	335	3 0 3 4 4	2 0 2 3 3
771786.8455	0.0000	−2.0349	3	25.7529	8	38001	335	3 0 3 4 4	2 0 2 3 4
771786.8637	0.0000	−2.0790	3	25.7533	10	38001	335	3 0 3 5 5	2 0 2 4 5
771789.5897	0.0000	−5.6801	3	25.7532	8	38001	335	3 0 3 5 4	2 0 2 2 3
771791.3481	0.0000	−7.9628	3	25.7533	6	38001	335	3 0 3 2 3	2 0 2 4 4
771791.3569	0.0000	−2.5796	3	25.7529	4	38001	335	3 0 3 3 2	2 0 2 3 3
771791.3688	0.0000	−2.5801	3	25.7529	8	38001	335	3 0 3 3 4	2 0 2 3 3
771791.3823	0.0000	−1.8579	3	25.7529	4	38001	335	3 0 3 3 2	2 0 2 3 2
771791.3864	0.0000	−1.5198	3	25.7529	8	38001	335	3 0 3 3 4	2 0 2 3 4
771791.3962	0.0000	−1.7203	3	25.7529	6	38001	335	3 0 3 3 3	2 0 2 3 3
771791.4072	0.0000	−6.1028	3	25.7533	6	38001	335	3 0 3 2 3	2 0 2 4 3
771791.4139	0.0000	−2.5763	3	25.7529	6	38001	335	3 0 3 3 3	2 0 2 3 4
771791.4216	0.0000	−2.5746	3	25.7529	6	38001	335	3 0 3 3 3	2 0 2 3 2
771791.4404	0.0000	−6.5360	3	25.7533	4	38001	335	3 0 3 2 2	2 0 2 4 3
771794.1552	0.0000	−2.3814	3	25.7532	2	38001	335	3 0 3 2 1	2 0 2 2 2
771794.1556	0.0000	−2.2746	3	25.7532	2	38001	335	3 0 3 2 1	2 0 2 2 1
771794.1818	0.0000	−2.3459	3	25.7532	6	38001	335	3 0 3 2 3	2 0 2 2 2
771794.1820	0.0000	−1.6244	3	25.7532	6	38001	335	3 0 3 2 3	2 0 2 2 3
771794.2150	0.0000	−1.9990	3	25.7532	4	38001	335	3 0 3 2 2	2 0 2 2 2

Table 7
(Continued)

Frequency[a]	Uncertainty[b]	I^{c}	D^{d}	E_{lower}[e]	g_{up}[f]	Tag[g]	QnF[h]	Qn_{up}[i]	Qn_{lower}[j]
771794.2152	0.0000	−2.3452	3	25.7532	4	38001	335	3 0 3 2 2	2 0 2 2 3
771794.2153	0.0000	−2.3801	3	25.7532	4	38001	335	3 0 3 2 2	2 0 2 2 1
771796.5767	0.0000	−6.7671	3	25.7529	8	38001	335	3 0 3 5 4	2 0 2 3 3
771796.5944	0.0000	−6.3778	3	25.7529	8	38001	335	3 0 3 5 4	2 0 2 3 4
771796.6565	0.0000	−7.5460	3	25.7529	10	38001	335	3 0 3 5 5	2 0 2 3 4
771801.1678	0.0000	−3.1604	3	25.7529	2	38001	335	3 0 3 2 1	2 0 2 3 2
771801.1689	0.0000	−3.6539	3	25.7529	6	38001	335	3 0 3 2 3	2 0 2 3 3
771801.1866	0.0000	−2.7452	3	25.7529	6	38001	335	3 0 3 2 3	2 0 2 3 4
771801.1944	0.0000	−5.1289	3	25.7529	6	38001	335	3 0 3 2 3	2 0 2 3 2
771801.2021	0.0000	−2.9559	3	25.7529	4	38001	335	3 0 3 2 2	2 0 2 3 3
771801.2276	0.0000	−3.6855	3	25.7529	4	38001	335	3 0 3 2 2	2 0 2 3 2

Notes.
[a] Calculated frequency in MHz.
[b] Calculated uncertainty of the line. If the line position is in units of MHz then uncertainty of the line is greater or equal to zero.
[c] Base 10 logarithm of the integrated intensity at 300 K in nm^2 MHz.
[d] Degrees of freedom in the rotational partition function (0 for atoms, 2 for linear molecules, 3 for non-linear molecules).
[e] Lower state energy in cm^{-1} relative to the lowest energy level in the ground vibrionic state.
[f] Upper state degeneracy: $g_{up} = g_I \times g_N$, where g_I is the spin statistical weight and $g_N = 2N + 1$ the rotational degeneracy.
[g] Molecule tag.
[h] Coding for the format of quantum numbers. $QnF = 100 \times Q + 10 \times H + N_{Qn}$; N_{Qn} is the number of quantum numbers for each state; H indicates the number of half integer quantum numbers; Qmod5, the residual when Q is divided by 5, gives the number of principal quantum numbers (without the spin designating ones).
[i] Quantum numbers for the upper state.
[j] Quantum numbers for the lower state.

REFERENCES

Albertsson, T., Semenov, D. A., Vasyunin, A. I., Henning, T., & Herbst, E. 2013, ApJS, 207, 27
Allamandola, L. J., Sandford, S. A., & Tielens, A. G. G. M. 1992, ApJ, 399, 134
Allen, M., & Robinson, G. W. 1977, ApJ, 212, 396
Amin, M. Y. 1996, EM&P, 73, 133
Asplund, M., Grevesse, N., Sauval, A. J., & Scott, P. 2009, ARA&A, 47, 481
Blake, G. A., Keene, J., & Phillips, T. G. 1985, ApJ, 295, 501
Cazaux, S., Cobut, V., Marseille, M., Spaans, M., & Caselli, P. 2010, A&A, 522, 74
Chakrabarti, S., & Chakrabarti, S. K. 2000a, A&A, 354, L6
Chakrabarti, S. K., & Chakrabarti, S. 2000b, InJPB, 74, 97
Chakrabarti, S. K., Das, A., Acharyya, K., & Chakrabarti, S. 2006a, A&A, 457, 167
Chakrabarti, S. K., Das, A., Acharyya, K., & Chakrabarti, S. 2006b, BASI, 34, 299
Cuppen, H. M., & Herbst, E. 2007, ApJ, 668, 294
Das, A., Acharyya, K., Chakrabarti, S., & Chakrabarti, S. K. 2008a, A&A, 486, 209
Das, A., Acharyya, K., & Chakrabarti, S. K. 2010, MNRAS, 409, 789
Das, A., & Chakrabarti, S. K. 2011, MNRAS, 418, 545
Das, A., Chakrabarti, S. K., Acharyya, K., & Chakrabarti, S. 2008b, NewA, 13, 457
Das, A., Majumdar, L., Chakrabarti, S. K., & Chakrabarti, S. 2013a, NewA, 23, 118
Das, A., Majumdar, L., Chakrabarti, S. K., Saha, R., & Chakrabarti, S. 2013b, MNRAS, 433, 3152
Dalgarno, A., de Jong, T., Oppenheimer, M., & Black, J. H. 1974, ApJL, 192, L37
de Graauw, Th., Helmich, F. P., Phillips, T. G., et al. 2010, A&A, 518, L6
Draine, B. T. 1978, ApJS, 36, 595
Emprechtinger, M., Caselli, P., Volgenau, N. H., Stutzki, J., & Wiedner, M. C. 2008, A&A, 493, 89
Federman, S. R., Cardell, J. A., van Dishoeck, E. F., Lambert, D. L., & Black, J. H. 1995, ApJ, 445, 325
Foresman, J. B., & Frisch, A. 1996, Exploring Chemistry with Electronic Structure (Pittsburgh, PA: Gaussian, Inc.)
Froebrich, D. 2005, ApJS, 156, 169
Hasegawa, T., Herbst, E., & Leung, C. M. 1992, ApJ, 82, 167
Herbst, E. 2006, in Springer Handbook of Atomic, Molecular, and Optical Physics, ed. G. W. F. Drake (New York: Springer), 561
Jura, M. 1974, ApJL, 190, L33
Keane, J. V., Boogert, A. C. A., Tielens, A. G. G. M., Ehrenfreund, P., & Schutte, W. A. 2001, A&A, 375L, 43
Leitch-Devlin, M. A., & Williams, D. A. 1985, MNRAS, 213, 295
Linsky, J. L., Diplas, A., Wood, B. E., et al. 1995, ApJ, 451, 335B
Lis, D. C., Pearson, J. C., Neufeld, D. A., et al. 2010, A&A, 521, L9
Majumdar, L., Das, A., & Chakrabarti, S. K. 2013a, A&A, in press (arXiv:1311.7543)
Majumdar, L., Das, A., Chakrabarti, S. K., & Chakrabarti, S. 2012, RAA, 12, 1613
Majumdar, L., Das, A., Chakrabarti, S. K., & Chakrabarti, S. 2013b, NewA, 20, 15
Müller, H. S. P., Schloder, F., Stutzki, J., & Winnewisser, G. 2005, JMoSt, 742, 215
Müller, H. S. P., Thorwirth, S., Roth, D. A., & Winnewisser, G. 2001, A&A, 370, L49
Myers, P. C., Adams, F. C., Chen, H., et al. 1998, ApJ, 492, 703
Neufeld, D. A., Goicoechea, J. R., Sonnentrucker, P., et al. 2010, A&A, 521, L10
Neufeld, D. A., Roueff, E., Sbell, R. L., et al. 2012, ApJ, 748, 37
Neufeld, D. A., & Wolfire, M. G. 2009, ApJ, 706, 1594
Pascual-Ahuir, J. L., Silla, E., & Tuñon, I. 1994, JCoCh, 15, 1127
Pickett, H. M. 1991, JMoSp, 148, 371
Pilbratt, G. L., Riedinger, J. R., Passvogel, T., et al. 2010, A&A, 518, L1
Puzzarini, C., Stanton, J. F., & Gauss, J. 2010, IRPC, 29, 273
Roberts, H., & Millar, T. J. 2000, A&A, 361, 388
Saito, S., & Yamamoto, S. 1988, JChPh, 88, 2281
Salez, M., Frerking, M. A., & Langer, W. D. 1996, ApJ, 467, 708
Schilke, P., Phillips, T. G., & Wang, N. 1995, ApJ, 441, 334
Shalabiea, O. M., & Greenberg, J. M. 1994, A&A, 290, 266
Smith, M. 1998, Ap&SS, 261, 169
Sonnentrucker, P., Neufeld, D. A., Phillips, T. G., et al. 2010, A&A, 521, L12
Stantcheva, T., Shematovich, V. I., & Herbst, E. 2002, A&A, 391, 1069
Su, T., & Chesnavich, W. J. 1982, JChPh, 76, 5183
Tomasi, J., Cammi, R., Mennucci, B., Cappelli, C., & Corni, S. 2002, PCCP, 4, 5697
Tomasi, J., Mennucci, B., & Cammi, R. 2005, ChRv, 105, 2999
Tomasi, J., Mennucci, B., & Cancés, E. 1999, JMoSt, 464, 211
van Dishoeck, E. F., & Black, J. H. 1986, ApJS, 62, 109
Woodall, J., Agndez, M., Markwick-Kemper, A. J., & Millar, T. J. 2007, A&A, 466, 1197
Woon, D. E., & Herbst, E. 2009, ApJS, 185, 273
Zmuidzinas, J., Blake, G. A., Carlstrom, J., et al. 1995, ApJL, 447, L125